Stabilization of 3d-transition metal hydrido complexes in $SrH_2Mg_2[Co(I)H_5]$, $BaH_2Mg_5[Co(-I)H_4]_2$ and $RbH_2Mg_5[Co(-I)H_4\ Ni(0)H_4]$ with a novel "back donation" mechanism

Henrik Fahlquist, David Moser, Dag Noréus, Keith Refson and Stewart F. Parker

Published version information

Citation: Fahlquist, H et al. "Stabilization of 3d transition metal hydrido complexes in SrH2Mg2[Co(I)H5], BaH2Mg5[Co(-I)H4]2, and RbH2Mg5[Co(-I)H4 Ni(0)H4] via easily polarizable hydride ligands." Inorganic Chemistry, vol. 55, no. 7 (2016): 3576-3582.

Stabilization of 3d-transition metal hydrido complexes in $SrH_2Mg_2[Co(I)H_5]$, $BaH_2Mg_5[Co(-I)H_4]_2$ and $RbH_2Mg_5[Co(-I)H_4\ Ni(0)H_4]$ with a novel "back donation" mechanism

Henrik Fahlquist,[1] David Moser,[1$] Dag Noréus,[1] Keith Refson[2,3] and Stewart F. Parker[3]

[1]Department of Materials and Environmental Chemistry, Arrhenius Laboratory, Stockholm University, S-106 91 Stockholm, Sweden

[2]Department of Physics, Royal Holloway, University of London, Egham TW20 0EX, UK

[3]ISIS Facility, STFC Rutherford Appleton Laboratory, Chilton, Didcot, Oxon OX11 0QX, UK.

$ Current address: Institute for Renewable Energy, EURAC, 39100 Bolzano, Italy

*S Supporting Information

Abstract

A combined study using neutron diffraction, inelastic neutron scattering and first principles calculations describe cobalt with a very low formal oxidation state of (-I) in a slightly distorted tetrahedral $Co(-I)H_4$-complex in $BaH_2Mg_5[Co(-I)H_4]_2$ and in the structurally related $RbH_2Mg_5[Co(-I)H_4\ Ni(0)H_4]$. This indicates that the electron "back donating" effect *via* the polarisable hydride ions to the counter ions in the solid state hydrides, can be compared to more conventional "back bonding" able to reduce the oxidation state down to -I. The hydrides were synthesised by hot sintering of transition metal powders with corresponding binary alkali- and alkaline earth hydrides. In the similarly synthesized $SrH_2Mg_2[Co(I)H_5]$, cobalt is formally +I-valent, showing a high sensitivity to differences in the counter ion framework, which can also influence electrical properties.

Introduction

If electropositive alkali and alkaline earth metals are reacted under hydrogen with transition metals (TM) to the right of group V, the TM is likely to form TM-hydrido complexes with the valence electrons from the electropositive metals. The bonding in the complexes has mainly an sd-electron character. This makes 4d- and 5d TM-hydrido complexes strong, since the soft 4d- and 5d orbitals are better suited to the very polarisable and soft hydride ions. The stability of the corresponding ternary hydrides becomes too high for practical applications; in addition these metals are prohibitively expensive. More interesting are the 3d TM-hydrido complexes. The 3d-electrons are not well suited to bonding with hydrogen and to stabilize the complexes, help is needed from a strongly polarizing counter ion *i.e.* Mg^{2+}.[1,2] A much investigated example is the $Mg_2[NiH_4]$ system. Several hundred papers have been written to date and the system still attracts interest for possible hydrogen storage. In $Mg_2[NiH_4]$, nickel forms an 18 electron, tetrahedral formally zero-valent $[Ni(0)H_4]^{4-}$ complex, with the help of the valence electrons from magnesium. However, the strongly polarizing Mg^{2+} has another significant influence on the electronic structure of this type of hydride. Without Mg in the counterion lattice, the electronic structures of the complexes are very "molecular like" and the bands can be easily identified with their molecular orbital counter parts, as they are essentially flat in the electronic density of states (eDOS).[2] With the strongly polarizing Mg^{2+} ion the bands become dispersed and overlapping. This implies unusual and interesting bonding properties making Mg_2NiH_4 interesting also from a fundamental solid state physics perspective. The central nickel atom is in an electron rich formal zero-valent d^{10} oxidation state. Such low oxidation states usually require strong electron accepting ligands, which can transfer some electron density from the central nickel atom by "back donation" to the ligand orbitals. In the solid state polarizing Mg^{2+} ions can relieve some of this electron density *via* the very polarisable hydride ion. This reduces the molecular character of the $[Ni(0)H_4]$-complex and makes the ternary hydride more stable, but also more metal-like. We have recently shown how subtle changes in the counter ion lattice have a profound influence on the electron conductivity, switching it from a conductor to an insulator with the help of a stacking fault in the lattice, that changes the band gap.[3] The stabilizing influence of the Mg^{2+} ions is, however, strong and the stability of $Mg_2[NiH_4]$ is still too high for any practical application to have evolved. In an effort to reduce the stability, trials to partially substitute the Mg^{2+} ions with less polarizing counter ions have been attempted.[4] However, few hydrides based on 3d-TM complexes have been synthesized

without having magnesium as a counter ion limiting the number of such hydrides found to date.

The purpose of the present paper was to investigate how other 18 electron hydrogen complexes based on cobalt, reacted to substitutions of Mg^{2+} ions with softer and less polarizing counter ions. A low formal oxidation state in a $[Co(-I)H_4]^{5-}$ complex could be stabilized in $BaH_2Mg_5[Co(-I)H_4]_2$ with the help of more electropositive and less polarizing Ba^{2+} ions. By substituting the Ba^{2+} ions with Rb^{+} ions, the structure can essentially be retained in $RbH_2Mg_5[Co(-I)H_4][Ni(0)H_4]$ if a corresponding number of $[Co(-I)H_4]^{5-}$complexes are substituted by $[Ni(0)H_4]^{4-}$ complexes. This indicates the importance of the electron count for forming these hydrides. In $SrH_2Mg_2[Co(I)H_5]$ the higher formal oxidation state of +I for cobalt is maintained, when Mg^{2+} is partly substituted by with Sr^{2+}, which is not as soft as Ba^{2+} and Rb^{+}.

The electron dense complexes are hydrogen rich with interesting electron conductivity properties related to how the lattice helps to relieve the high electron density in the complexes. We believe that the complexes are interesting for both their electronic structure and their high hydrogen contents.

Experimental

Synthesis

All starting materials and samples were handled inside a continuously purified argon filled glove box. Heat treatment was done by placing pressed pellets of ground powders in aluminium oxide tubes heated in stainless steel reactors placed in a tube furnace. The temperature was monitored by contacting a thermocouple in a sealed stainless steel capillary to the sample.

BaH_2 was made by reacting barium pieces from Sigma Aldrich to 573 K in 20 bar H_2 atmosphere overnight yielding brittle, white pieces of BaH_2. Mg_2CoH_5 was made by heat treatment of pelletized MgH_2 and Co metal powders in the molar ratio 2:1 in 70 bar of H_2 at 773 K for 18 hours, resulting in black Mg_2CoH_5.

Mg_2NiH_4 was produced by reacting pulverized Mg_2Ni alloy in a 40 bar H_2 atmosphere at 623 K. The hydride was cycled five times by releasing and restoring the hydrogen pressure over a period of 8 hours to obtain a fully hydrogenated brown sample.

$BaH_2Mg_5[CoH_4]_2$ was made by mixing BaH_2, Mg_2CoH_5 and MgH_2 in the molar ratio 1:2:1 using a pestle and mortar. The powder mixture was pelletized and heat treated in 70 bar H_2 at 833 K for 18 hours. The resulting product was a single phase black powder.

$RbH_2Mg_5[CoH_4][NiH_4]$ was made by mixing Rb, Mg_2CoH_5, Mg_2NiH_4 and MgH_2 in the molar ratio 1:1:1:1 using a pestle and mortar. The powder was pelletized and heat treated in 70 bar H_2 at 773 K for 18 hours. The resulting product was a single phase dark purple powder.
$Ba_{0.5}Rb_{0.5}H_2Mg_5[CoH_4]_{1.5}[NiH_4]_{0.5}$ was prepared in the same way as $RbH_2Mg_5[CoH_4][NiH_4]$ to yield a single phase black powder.

$SrH_2Mg_2[CoH_5]$ was made by mixing powders of SrH_2 and MgH_2 and Co powder in the molar ratio 1:2:1. The powder mixture was ground to a fine powder using a pestle and mortar and pelletized and heat treated in 70 bar H_2 at 815 K for 18 hours. The resulting product was an almost single phase black powder. To establish the optimum reaction conditions and reactant ratios given above, a rather time consuming trial and error procedure was required, where the reaction conditions were varied and after each run a small sample was removed for XRD analysis. To produce samples for neutron diffraction, deuterated analogues were produced using the corresponding deuterides and D_2 gas.

Structural investigations

X-ray diffraction patterns were obtained on a Panalytical X'pert pro powder diffractometer equipped with a germanium [111] monochromator (λ=1.540598 Å). Indexing of the unit cells were performed using the TREOR[5] feature in the software Panalytical Highscore Plus. From systematic extinctions, the unit cell of $BaH_2Mg_5[CoH_4]_2$ was assigned to the space group *Immm* (no. 71) by choosing the highest symmetry body centred space group. The unit cell was then refined in Panalytical Highscore Plus by least squares with resulting refined lattice parameters a= 7.392(2) Å, b= 11.602(4) Å, c= 4.6265(9) Å. For $RbH_2Mg_5[CoH_4][NiH_4]$, the lattice parameters were refined to a=7.345(6) Å, b=11.877(8) Å and c=4.703(3) Å and the structure was also initially assigned to the space group *Immm* (no. 71). The initial structures were solved in FOX[6] and the metal atom parameters were refined in Fullprof2000.

The least squares refinement of $RbH_2Mg_5[CoH_4][NiH_4]$ indicated a lower symmetry and the space group had to be changed to *Imm2* (no. 44), the final agreement factors were R_{wp}=0.0312 and R_p=0.0207 for the X-ray structure refinement.
The diffraction pattern for $SrH_2Mg_2[CoH_5]$ was indexed with a monoclinic cell with lattice parameters a=7.818(2) Å, b=4.462(1) Å, c=6.640(2) Å and β=91.27(2)º and the space group *C2/m*(no. 12) was assigned from extinction criteria and choosing the highest symmetry.

To elucidate the hydrogen positions, neutron powder patterns were obtained from the corresponding deuterides at the time-of-flight instrument GEM at ISIS using a sealed

cylindrical ø=5 mm vanadium sample holder. The initial deuterium positions were obtained using simulated annealing in FOX[6] keeping the metal positions fixed. The full structure refinement was performed by least squares refinement in GSAS[7].

The unit cell for $BaD_2Mg_5[CoD_4]_2$ was refined to a=7.39919 Å, b=11.570691 Å and c=4.622355 Å, slightly smaller than the hydride indicating anharmonic hydrogen vibrations that are commonly observed in these types of hydrides. R_{wp}=0.0223 and R_p=0.0165 for the full structure refinement. The structure with well separated and aligned but slightly distorted tetrahedral CoD_4 complexes is shown in Figure 1. The complexes nearest neighbours are all Mg^{2+} ions whereas the Ba^{2+} ions are found in "BaH_2" related layers separating "$Mg_5[CoD_4]_2$" layers.

The structure of $RbMg_5[CoD_4][NiD_4]$ was found to be closely related to that of $BaH_2Mg_5[CoD_4]_2$. Due to problems with a disordered arrangement of the Co- and Ni-complexes and a lower symmetry, the detailed structure could not be elucidated at this point. The metal atom positions could, however, be refined and the main difference to the metal atom structure in $BaH_2Mg_5[CoD_4]_2$ is a slight shift of the (2b) magnesium atom position at (0, 0 ½). A The shift is illustrated in Figure S1 of the Supporting Information. Table S3a lists the metal atom positions for $RbMg_5[CoD_4][NiD_4]$. Table S3b shows that partial substitutions of alkaline earth/alkali- metal and transition metals could be made leading to a continuous transition between the structures, if the 18-electron count is kept for the complexes.

The magnesium atom shift cannot be accommodated in the centrosymmetric space group *Immm* (no. 71), however, and the use of the non-centrosymmetric space group *Imm2* (no. 44) unfortunately increases the number of structural parameters to be refined, leading to instability problems in the refinements. Constraining the parameters can improve the stability but the result would be biased. The general picture is, however, that the tetragonal complexes are kept but their orientations are more disordered than the uniform alignment in the $BaH_2Mg_5[CoD_4]_2$ structure. Below it will also be shown that this leads to a smearing out of the vibrational frequencies in $RbMg_5[CoH_4][NiH_4]$ compared to $BaH_2Mg_5[CoH_4]_2$ although both exhibit similar general features.

The unit cell for $SrD_2Mg_2[CoD_5]$ was refined to a=7.8140(3) Å, b=4.4593(2) Å, c=6.6347(2) Å and β=91.237(3)°. Systematic absent reflexions in the XRD pattern indicated a C-centred symmetry but in the neutron diffraction pattern this was broken and space group $P12_1/n1$ (no. 11) was used for the neutron diffraction refinement of the deuteride. The agreement factors became R_{wp}=0.0378 and R_p=0.0297, for the full structure refinement.

The contents of the unit cell are illustrated in Figure 2. (Note that the structure of the hydride and the deuteride are the same when the hydrogen positions are included). The crystallographic results of all the complexes studied are summarised in Table 1 and selected distances can be found in Table 2. A more complete set is given in Tables S1 – S5 of the Supporting Information.All hydrides contain hydrogen both in interstitial sites and bound in complexes.

Calculations - CASTEP

Periodic DFT calculations of the crystalline structures were carried out using the plane-wave pseudopotential method implemented in the CASTEP code.[8,9] Exchange and correlation were approximated in the local density approximation (LDA) using the CA-PZ[10,11] parameterization. Optimized norm-conserving pseudopotentials[12] were used with a plane-wave cut-off of 990 eV. The equilibrium structure, an essential prerequisite for lattice dynamics calculations was obtained by BFGS geometry optimization after which the residual forces were converged to zero within 0.009 eV/Å. Spin polarised calculations were carried out for all the complexes considered by computational methods. All produced diamagnetic ground states. Electronic densities of states were generated from a subsequent band structure calculation using OptaDOS.[13] Phonon frequencies were obtained by diagonalisation of dynamical matrices computed using density-functional perturbation theory[9,14] (DFPT). To reduce the computational expense, these calculations were carried out on non-spin polarised systems. An analysis of the resulting eigenvectors was used to map the computed modes to the corresponding irreducible representations of the point group and assign IUPAC symmetry labels. In addition to the direct evaluation of frequencies and intensities at zero wavevector, phonon dispersion was calculated along high symmetry directions throughout the Brillouin zone. For this purpose, dynamical matrices were computed on a regular grid of wavevectors throughout the Brillouin zone and Fourier interpolation was used to extend the computed grid to the desired fine set of points along the high-symmetry paths.[14] The program ACLIMAX[15] was used to produce the INS spectrum from the *ab initio* results.

While the LDA gave reasonable predictions of vibrational frequencies, there was some sensitivity to the choice of XC functional. Calculations carried out with generalized gradient approximation (GGA) using the PBE functional[16] resulted in imaginary frequencies for some vibrational modes, indicating a structural instability, while LDA gave all-real frequencies and no instability. As in other cases with mixed covalent/Van der Waals interactions, it is likely that this stabilisation is the result of a cancellation of error between the well-known LDA

overbinding and the omission of Van der Waals forces from both LDA and GGA. For purposes of mode assignment and interpretation of experimental spectra, this approximation is tolerable and only LDA results are presented below.

Inelastic neutron scattering

INS spectra[17] were obtained with the spectrometers TOSCA[18] and MAPS[19] at ISIS.[20] The instruments are highly complementary: TOSCA has excellent resolution at <1400 cm^{-1} while MAPS provides access to higher energy transfer. Incident energies (E_i) of 4033 and 2420 cm^{-1} were used. For the INS measurements the samples were loaded into indium wire sealed aluminium cans in a glovebox. The spectra were recorded at <20 K for 7-10 hours. INS spectroscopy[17] has several advantages that make it valuable for the study of complex metal hydrides.[21] The spectral intensity, $S(Q,\omega)$, depends on the product of the incoherent cross section and the amplitude of vibration of the atoms in the mode. Hydrogen, ^1H, is both the lightest element (hence has the largest amplitude of vibration) and has the largest cross section, thus motions that involve hydrogen will dominate the spectrum. Further, since the scattering is purely dynamic, the symmetry requirements resulting from the interaction of light with electrons that give rise to selection rules for infrared and Raman spectroscopies are absent and all modes are allowed.

Results and Discussion.

In $Mg_2[CoH_5]$, a $Co(I)H_5$ complex with a square-based pyramidal structure[22] is surrounded by magnesium counter ions and the formal cobalt oxidation state is +1. By substituting some of the magnesium with the more electropositive and less polarizing barium the formal oxidation state was reduced to a surprisingly low -1 in $BaH_2Mg_5[Co(-I)H_4]_2$. In our DFT calculations this increased the band gap from 0.3 eV to close to 1 eV, Figure 3 and Figure S2. The barium could be further substituted by rubidium but in order to keep the electron count correct for the 18 electron complexes, cobalt has also to be partly substituted by nickel. This led to $RbH_2Mg_5[Co(-I)H_4][Ni(0)H_4]$ with a structure closely related to that of $BaH_2Mg_5[Co(-I)H_4]_2$. It is further possible to continuously move between these limiting compositions (Table S3a and b). Due to the disorder in the structure no DFT calculation was performed. But the colour change from black to dark red with increasing Rb content indicates an increasing band gap.

In $SrH_2Mg_2[CoH_5]$ the DFT calculation shows a decreased band gap of 0.1 eV, Figure 4. In contrast to the Ba hydride, the band gap is indirect. The optical gap is 1.2 eV; see Figure

S3. This was also corroborated by a simple measurement of the electric resistivity using a standard Ohmmeter. Pressed tablets of $SrH_2Mg_2[CoH_5]$ are conducting at room temperature. However, if the temperature is reduced by cooling the tablet with liquid nitrogen, the measurable conductivity disappears but is restored when the temperature is increased.

The partial density of states clearly show different crystal field splitting of the 3d-orbitals for the Ba (tetrahedral Co) and Sr (square-based pyramidal) hydrides, with the lower energy part of the 3d-orbital manifold overlapping with the hydrogen 1s orbitals in a bonding interaction. For $SrH_2Mg_2[CoH_5]$, the Co 3d-orbitals account for most of the total density of states between -3 and 0 eV. For $BaH_2Mg_5[Co(-I)H_4]_2$, this is not the case and there is significant overlap with the Mg orbitals, consistent with a degree of covalent bonding between Mg and Co. The difference between the Sr and Ba hydrides is probably because the closest M-to-Co distance is 2.686 for M = Sr, but 2.430 for M = Ba.

Tables 2 and S1, S2, S4 and S5 include the calculated structural parameters for $BaH_2Mg_5[Co(-I)H_4]_2$ and $SrH_2Mg_2[Co(I)H_5]$. Corresponding tables for $Mg_2[Co(I)H_5]$ are included in the Supporting Information (Tables S6 and S7). It can be seen that in all cases the calculated values are very close to those observed experimentally: bond distances are all within 0.1 Å and bond angles are generally within a few degrees. For all the complexes there is a tendency that the variation in bondlengths is less marked in the calculations than is observed experimentally, although the trends are always correct, *e.g.* for $SrH_2Mg_2[Co(I)H_5]$ the observed Co–H distances are 1.65 and 1.52 Å, while the calculated distances are 1.603 and 1.566 Å. These distances are also slightly longer than are found (experimentally[21] and computationally) in $Mg_2[Co(I)H_5]$.

CASTEP calculations of the Born effective charges, (defined as the electric polarization generated upon displacement of an atom, thus are dynamical charges) of the $[CoH_x]$ units yield almost identical values with diagonal components (-4.0,-4.0, -3.9) [Mg] and (-4.1,-4.0,-3.5)[Sr] in these two cases, also indicating very similar electronic environments. By contrast with static population analysis the Born charges characterize the electron dynamics and are usually close to formal ionic charges. The effective charge on the corresponding cations is +2.2 [Mg] and +2.3 [Sr]. Surprisingly, the barium complex that contains $[Co(-I)H_4]^{5-}$ ions has similar stretching energies, Figure 5, despite the cobalt being in a lower oxidation state. In that case the Born effective charges are slightly more negative at (-4.5,-4.8, -4.7) on $[Co(-I)H_4]$, close to the formal -5, with +2.8 on Ba. The electropositive counterions push different degrees of electrons on to the complexes, but the polarizing Mg^{2+} ions can help to redistribute the electrons *via* the hydrogen atoms.

A static Hirshfeld population analysis from the DFT calculations supports these trends, despite yielding results much smaller than the formal ionic charge states. (A significant difference between the magnitudes of calculated static and dynamic charges is well-documented[23,24]). Ba and Sr get a similar Hirshfeld charge of +0.29 e in both hydrides. Co(-I) and Co(+I) get -0.33 and -0.29 e, respectively. The interstitial hydrogen atoms are more ionic with a charge of -0.15 e in both compounds compared to the hydrogen in the contingent complexes, which have a charge of -0.07 and -0.09 in the Co(+I) and Co(-I) complex, respectively. Finally the magnesium atoms in the Co(-I) hydride are less positive with a Hirshfeld charge of 0.29 e compared to 0.32 e for the Co(+I) hydride. The delicate balance of these electron redistributions seems to be intricately dependent on the size and electropositivity of the counter ions. It is interesting, however, that the formal oxidation state has greater implication for more subtle effects such as the band gap. Both $Mg_2Co(I)H_5$ and $SrH_2Mg_2[Co(I)H_5]$ have very small bandgaps and are more metallic than $BaH_2Mg_5[Co(-I)H_4]_2$ and also $RbH_2Mg_{10}[Co(-I)H_4\ Ni(0)H_4]$ both with bandgaps greater than 1 eV.

Figure 5 compares the INS spectra of the three compounds recorded on TOSCA. It can be seen that while $SrH_2Mg_2[Co(I)H_5]$ and $BaH_2Mg_{10}[Co(-I)H_4]_2$ give well-resolved spectra while the mixed complex $RbH_2Mg_{10}[Co(-I)H_4\ Ni(0)H_4]$ gives very broad bands with little hint of any structure, consistent with the disorder present.

Figure 6 shows the INS spectra of $BaH_2Mg_{10}[Co(-I)H_4]_2$ recorded on MAPS. The lower part is obtained by summing over the momentum transfer with two different incident energies. With E_i = 2420 cm^{-1} the Co–H stretching modes at 1678 and 1788 cm^{-1} are easily observed, while with E_i = 4033 cm^{-1} two weak bands at 3287 and 3517 cm^{-1} with a shoulder at 3466 cm^{-1} are apparent. These are assigned as the first overtone of each of the stretching modes and the combination mode respectively and clearly there is significant anharmonicity present since the predicted overtones would be at 3356 and 3576 cm^{-1}. This is consistent with the difference in unit cell parameters of the hydrides and deuterides.

The spectra can be summarized as: M–H stretching modes 1600 - 1900 cm^{-1}, H–M–H bending modes and H^- translations 700 – 1200 cm^{-1}, complex ion librational modes 350- 700 cm^{-1} and heavy atom translation modes (acoustic and optic) 0 – 350 cm^{-1}. To go beyond this simple description, additional information is required which can be obtained from the CASTEP *ab initio* calculations.

For $BaH_2Mg_5[Co(-I)H_4]_2$ and $SrH_2Mg_2[Co(I)H_5]$ the CASTEP calculations show that there is significant variation in transition energy with wavevector (dispersion)in the modes as shown by the dispersion curves, Figures S4 and S5 (the discontinuities at the Γ-point, (0,0,0),

are due to “LO-TO” splitting). By comparison of the observed and calculated spectra, Figures S6 and S7, it can be seen that the spectra generated from the calculation across the entire Brillouin zone are in much better agreement with the experimental spectra than those from a calculation at just the Γ-point. This is a consequence of the interaction of neutrons with phonons of all momentum transfers, not just at Q ~0 as for infrared and Raman spectra. The long range interactions evidenced by the spectra emphasise the need for fully periodic calculations in metal hydride systems. The interaction is most likely to be the result of the Coulombic interactions between the ions as was found for $Ba[ReH_9]$.[25] Animations of the modes enables assignments to be made and these are given in the supporting information for the Γ-point modes of $BaH_2Mg_5[Co(\text{-I})H_4]_2$ and $SrH_2Mg_2[Co(I)H_5]$ respectively.

Since the INS spectrum is purely dynamic, we can investigate the contributions of the individual species separately. By setting the cross-section of all the atoms to zero, except for the atoms of interest, only the modes involving motion of those atoms will contribute to the calculated INS spectrum, as depicted in Figures 7 and 8**.** Thus for $BaH_2Mg_5[Co(\text{-I})H_4]_2$ the $[Co(\text{-I})H_4]^{5-}$ ion has translational modes below 200 cm^{-1}, librational modes around 400 cm^{-1}, H–Co–H bending modes at 500 – 700 cm^{-1} and Co–H stretching modes at 1650 – 1850 cm^{-1}. If the cobalt atom is considered in isolation then the pattern looks very similar except that there is very little intensity in the librational region as expected since, to a first approximation, the centre of mass is invariant during a libration. The interstitial hydrogen atoms exhibit relatively pure modes at 600 – 750 cm^{-1} and 900 – 1000 cm^{-1} and account for most of the intensity in this region. The translational modes of the magnesium ions are all at < 450 cm^{-1} with those of the barium ion largely below 200 cm^{-1}. As expected, below 450 cm^{-1} there is significant mixing of modes and there are no pure modes.

A similar pattern is found for $SrH_2Mg_2[Co(I)H_5]$, Figure 8, with the Sr^{2+}, Mg^{2+} and H^- modes at energies close to those found in the barium containing compound. The librational and deformational modes of the complex ion occur at somewhat higher energies than those found in the barium containing compound: librations at 500 – 700 cm^{-1}, H–Co–H bending modes at 700 – 1000 cm^{-1} while the Co–H stretching modes at 1600 – 1850 cm^{-1} are at comparable energies.

Figure 9a and 9b compare the experimental INS spectrum of $Mg_2[Co(I)H_5]$[26] and that of the $[Co(I)H_5]^{4-}$ ion in $SrH_2Mg_2[Co(I)H_5]$ generated by considering only the hydrides bonded to the cobalt. The degree of similarity is remarkable; the only significant difference is that the librational modes in the strontium complex are 10 – 20% higher in energy than in the parent compound. The similarity in the transition energies of the stretching modes would indicate

that the bonds are also of similar strength, although the degeneracies are lifted, Figure 9c, by virtue of the site symmetry; C_s *vs*. C_{4v}.

Conclusions

We have used a combination of diffraction, spectroscopic and computational methods to characterise the structure and bonding of the novel transition metal hydrides: $SrH_2Mg_2[Co(I)H_5]$, $BaH_2Mg_5[Co(-I)H_4]_2$ and $RbH_2Mg_5[Co(-I)H_4\ Ni(0)H_4]$. The complexes can be considered as derivatives of $Mg_2[Co(I)H_5]$. The results show that the band gap depends sensitively on the nature of the alkaline earth cations present. In the Ba hydride the band gap is considerably reduced from that of $Mg_2[Co(I)H_5]$ and further reduced in the Sr hydride. However, in the latter case, the band gap is indirect. The direct gap is comparable to that of the Ba hydride. Despite the difference in formal oxidation state of the Co in the Sr (Co(+I)) and Ba (Co(-I)) complexes, the INS spectra and the electronic structure calculations point to a close similarity in the electronic structures of the cobalt complexes in both compounds. The similarity of the transition energies of the stretching modes in the Rb complex would suggest that this is also the case here. Overall, the results show that it is possible to manipulate the electronic properties of complex metal hydrides by an appropriate choice of counter ion, and that the electron "back donating" effect via the polarisable hydride ions to the counter ions in the solid state hydrides, can be compared to more conventional "back bonding" able to reduce the oxidation state down to -I. But there are only minor differences between the formal low spin d^8 Co(+I) in the Sr hydride and the d^{10} Co(-I) in the Ba and Rb hydrides.

■ ASSOCIATED CONTENT

*S Supporting Information

The Supporting Information is available free of charge on the ACS Publications website at DOI:

Crystallographic data and interatomic distances and angles for the complexes (seven tables), observed and calculated Γ-point transition energies for the Ba and Sr complexes (two tables). A pictorial view of the magnesium displacement in the Rb complex (one figure), vibrational dispersion curves for the Ba and Sr complexes (two figures) and comparison of observed and calculated INS spectra for the Ba and Sr complexes (two figures) (PDF).

Acknowledgements

The STFC Rutherford Appleton Laboratory is thanked for access to neutron beam facilities. Computing resources (time on the SCARF computer used to perform the CASTEP calculations) was provided by STFC's e-Science facility. This work has been financially supported the Swedish Energy Agency.

Tables

Table 1. Lattice parameters, space groups and lattice parameters for the investigated compounds.

Compound	$BaH_2Mg_5[Co(-I)D_4]_2$	$RbH_2Mg_5[CoH_4][NiH_4]$	$SrH_2Mg_2[CoD_5]$
Space group, Z	*Immm*, 2	*Imm2*, 2	$P12_1/n1$, 2
a, Å	7.392(2)	7.345(6)	7.818(2)
b, Å	11.602(4)	11.877(8)	4.462(1)
c, Å	4.6265(9)	4.703(3)	6.640(2)
β, deg	-	-	91.27(2)
R_p, %	1.65	2.07	2.97
R_{wp}, %	2.23	3.12	3.78

Table 2. Selected bond distances (Å) for the investigated compounds.

	$BaH_2Mg_5[Co(-I)H_4]_2$	$RbH_2Mg_5[CoH_4][NiH_4]$	$SrH_2Mg_2[CoH_5]$
Co–H	1.504 (×2), 1.605 (×2)		1.65, 1.52 (×2), 1.55 (×2)
Mg···H_{int}	2.090		1.950
AE···H_{int}	2.772		2.641
Mg···Co	2.430		2.686
AE···Mg	3.700		3.554

H_{int} = interstitial hydride. AE = Sr or Ba.

Figures

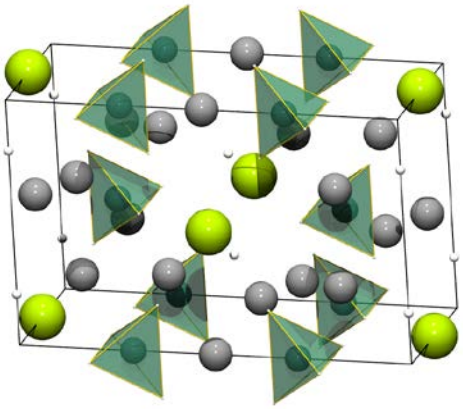

Figure 1**.** $BaD_2Mg_5[Co(-I)D_4]_2$ Z=2. $[Co(-I)D_4]$ are represented as green tetrahedra, Ba as lime green spheres and Mg as grey spheres.

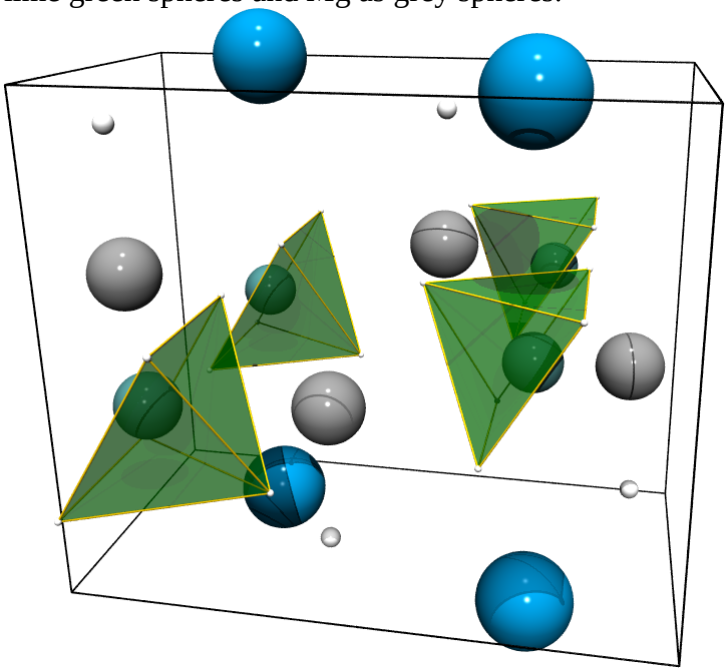

Figure 2. Structure of $SrD_2Mg_2[Co(II)D_5]$ Z=2. $[Co(II)D_5]$ are represented as green square pyramids, Sr as blue spheres and Mg as grey spheres

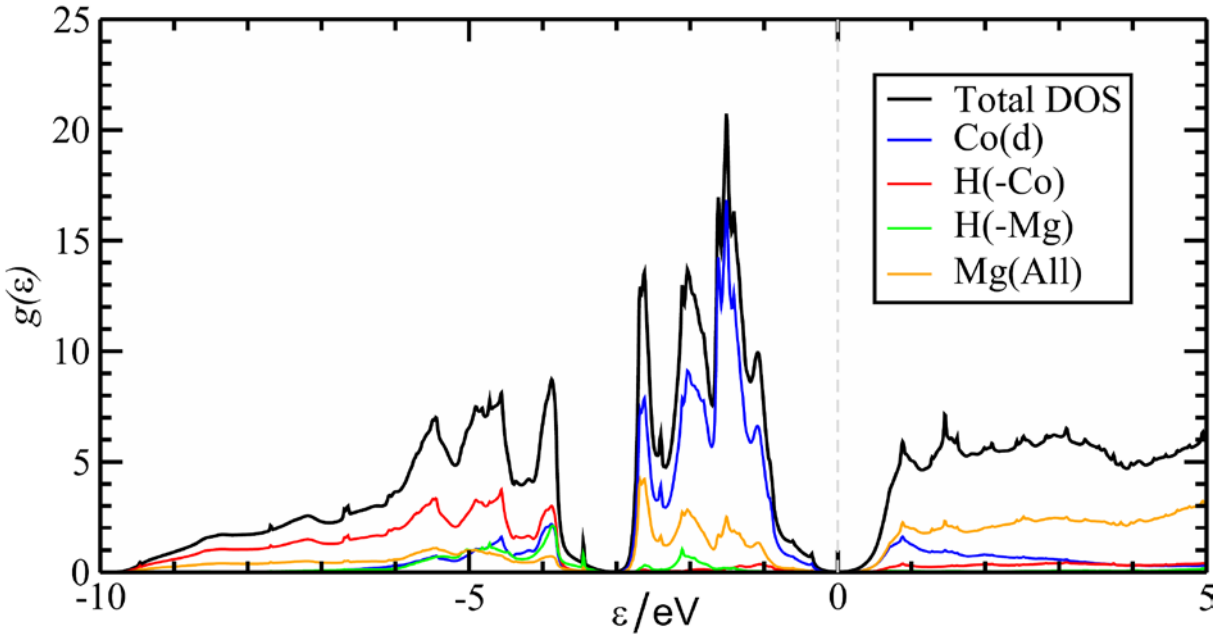

Figure 3. Electronic density of states (g(ε)) of $BaH_2Mg_{10}[Co(-I)H_4]_2$ (black). The partial density of states for the cobalt d-orbitals (blue) and the hydrogen atoms bonded to the cobalt (red) and the interstitial hydrogens (green) are also shown.

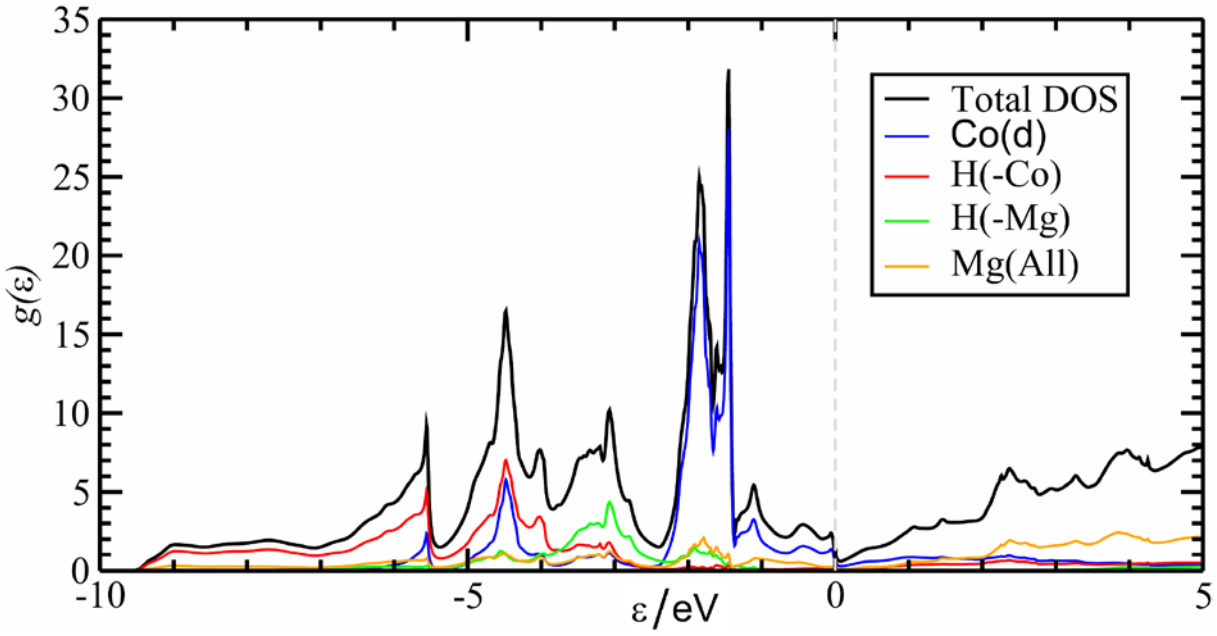

Figure 4. Electronic density of states (g(ε)) of $SrH_2Mg_2[Co(-I)H_5]$ (black). The partial density of states for the cobalt d-orbitals (blue) and the hydrogen atoms bonded to the cobalt (red) and the interstitial hydrogens (green) are also shown

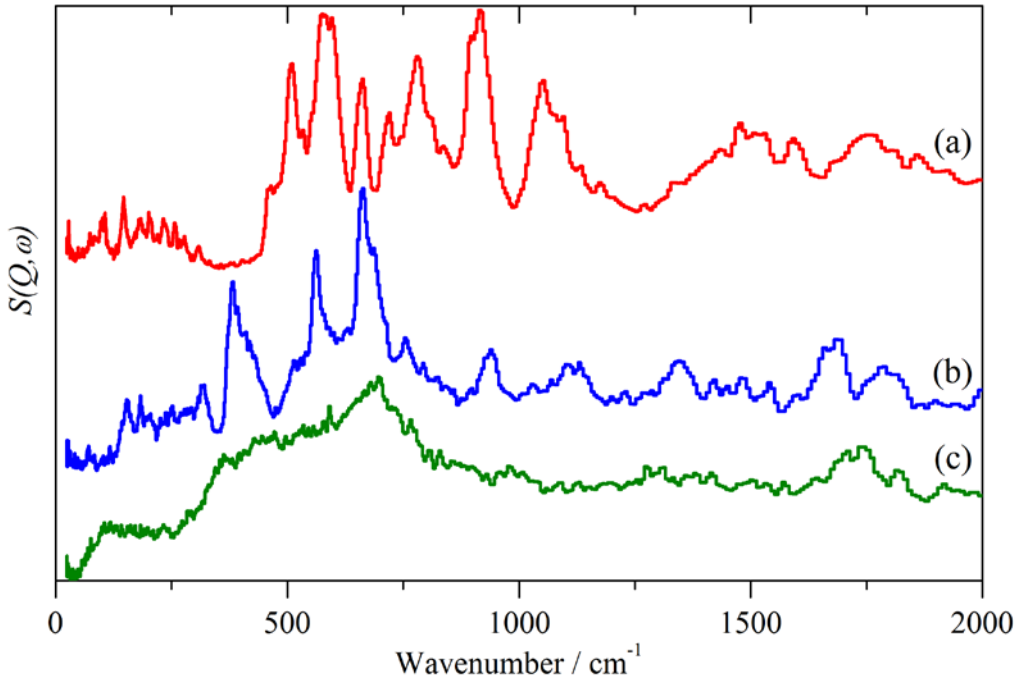

Figure 5. INS spectra recorded on TOSCA at 10 K of: (a) $SrH_2Mg_2[Co(I)H_5]$, (b) $BaH_2Mg_{10}[Co(\text{-}I)H_4]_2$ and (c) $RbH_2Mg_{10}[Co(\text{-}I)H_4\ Ni(0)H_4]$.

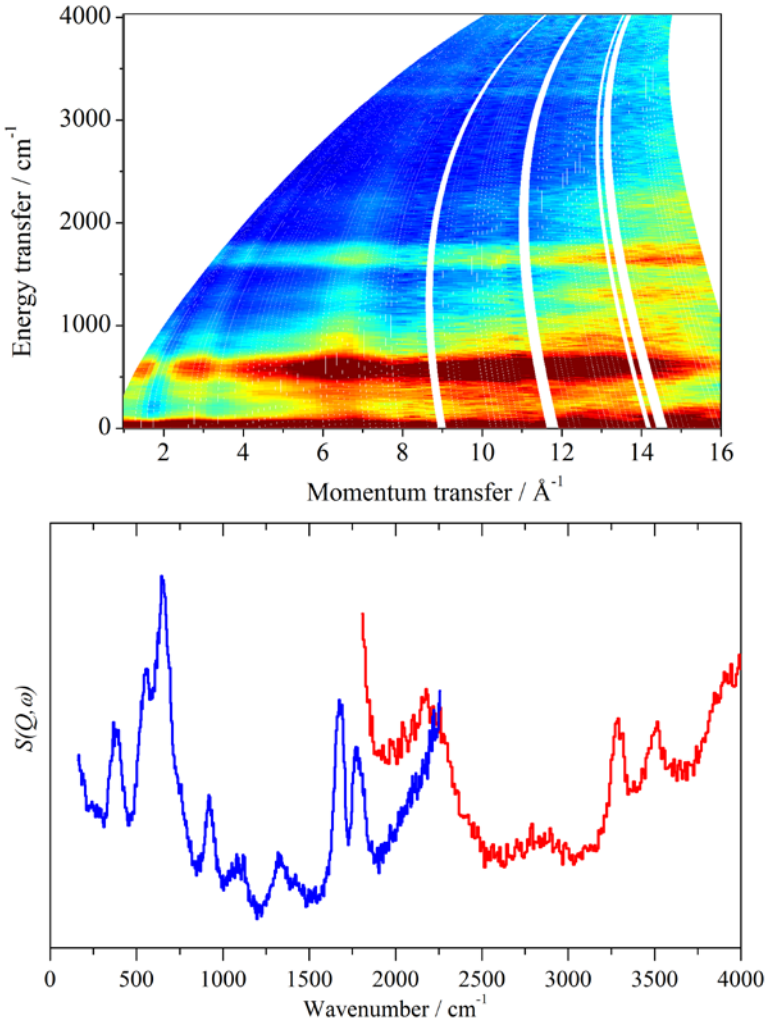

Figure 6. INS spectra recorded on MAPS at 10 K of $BaH_2Mg_{10}[Co(\text{-}I)H_4]_2$. Upper: *S(Q,ω)* map ($E_i$ = 4033 cm^{-1}). Lower: MAPS spectra obtained by summing over momentum transfer for E_i = 2420 cm^{-1} (blue trace) and E_i = 4033 cm^{-1} (red trace). The red trace is ×4 ordinate expanded relative to the blue trace.

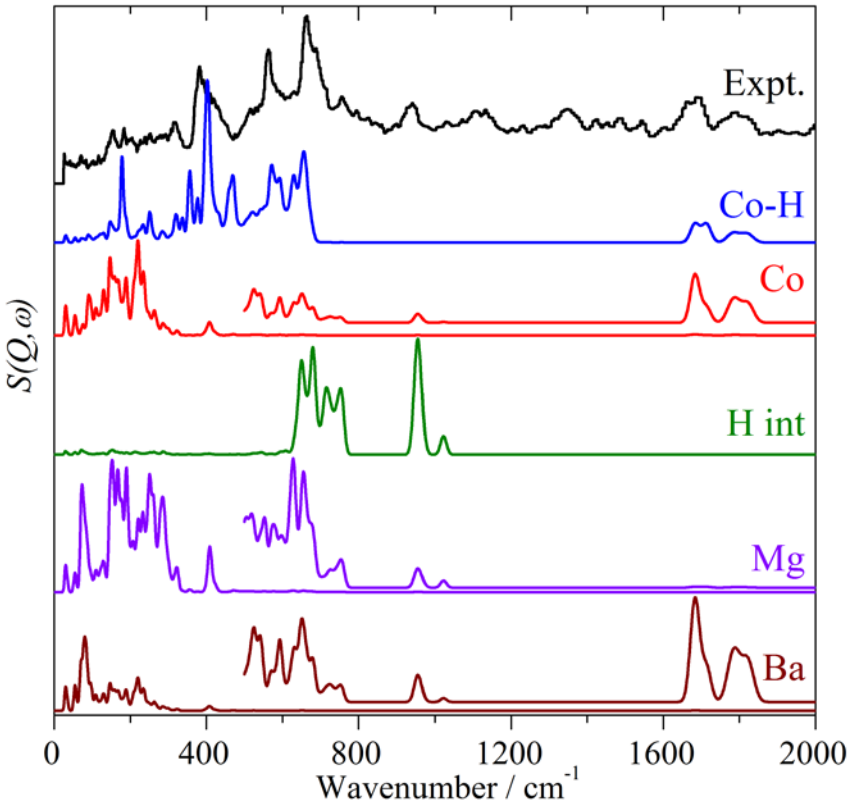

Figure 7. Comparison of the experimental (Expt., black) INS spectrum of $BaH_2Mg_5[Co(-I)H_4]_2$ with those generated by including only the motions of the hydrides bonded to the cobalt (Co–H, blue), the cobalt atoms (Co, red), the interstitial hydrides (H int, olive), the magnesium ions (Mg, violet), and the barium ions (Ba, brown). The insets in the spectra of Co, Mg and Ba are ordinate expansions of the region 500 – 2000 cm^{-1} with factors of 50, 80 and 300 respectively.

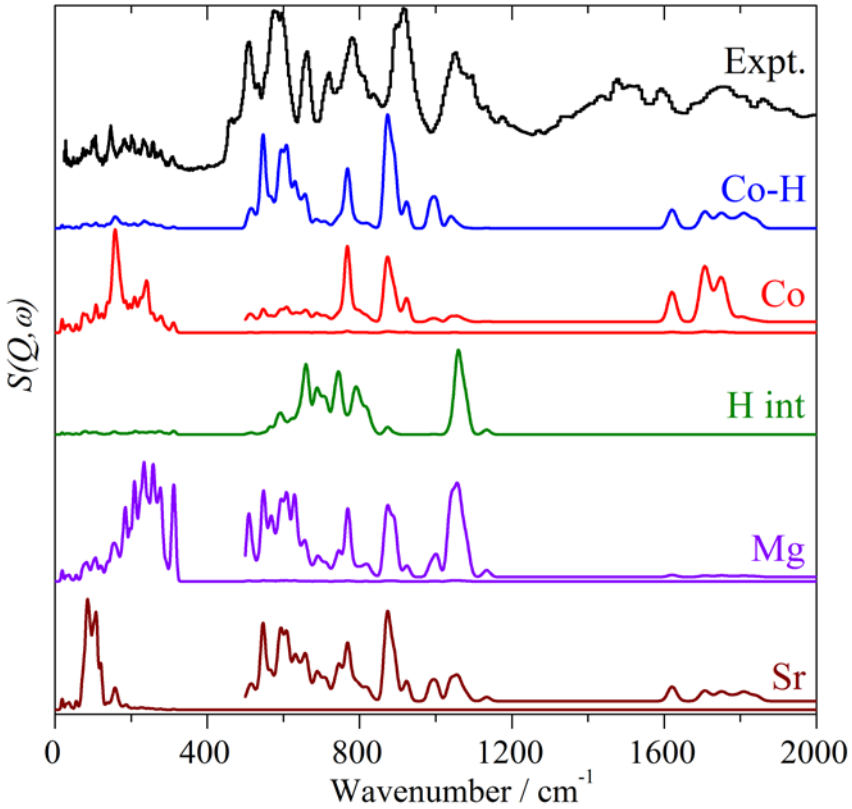

Figure 8. Comparison of the experimental (Expt., black) INS spectrum of $SrH_2Mg_2[Co(I)H_5]$ with those generated by including only the motions of the hydrides bonded to the cobalt (Co–H, blue), the cobalt atoms (Co, red), the interstitial hydrides (H int, olive), the magnesium ions (Mg, violet), and the strontium ions (Sr, brown), only the $0 \rightarrow 1$ transitions are shown. The insets in the spectra of Co, Mg and Ba are ordinate expansions of the region 500 – 2000 cm^{-1} with factors of 50, 100 and 400 respectively.

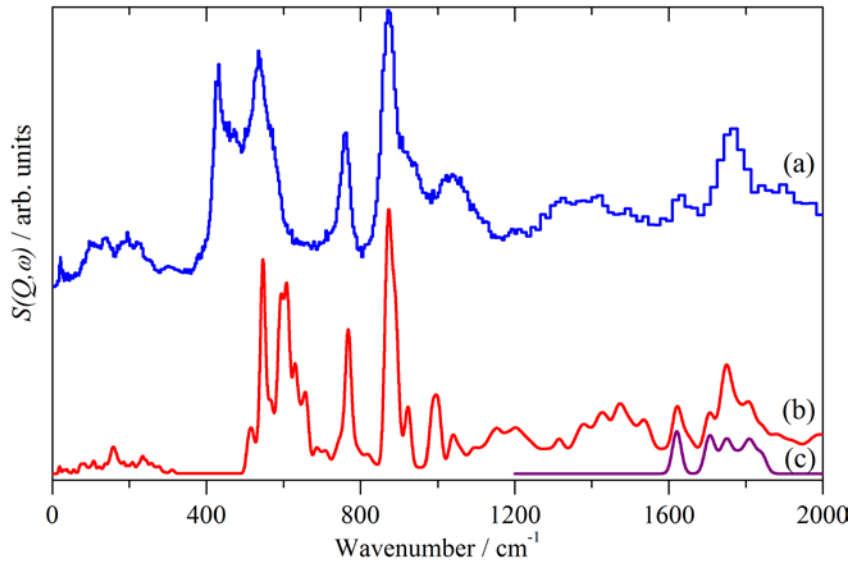

Figure 9. Comparison of the (a) experimental INS spectrum of $Mg_2[Co(I)H_5]$ and (b) that of the $[Co(I)H_5]^{4-}$ in $SrH_2Mg_2[Co(I)H_5]$ generated by considering only the hydrides bonded to the cobalt. To aid the comparison all transitions ($0 \rightarrow 1$, $2 \cdots 10$) are included, (c) as (b) but only the $0 \rightarrow 1$ transitions for the 1200 – 2000 cm^{-1} region are shown.

References

(1) Miller, G. J.; Deng, H.; Hoffmann, R. *Inorg. Chem.* **1994**, *33*, 1330–1339.

(2) Häussermann, U.; Blomqvist, H.; Noréus, D. *Inorg. Chem.* **2002**, *41*, 3684–3692.

(3) Lelis, M.; Milcius, D.; Wirth, E.; Hålenius, U.; Eriksson, L.; Jansson, K.; Kadir, K.; Ruan, J.; Sato, T.; Yokosawa, T. *J. Alloys Compd.* **2010**, *496*, 81–86.

(4) Kadir. K.; Noréus D.; Inorg. Chem. **2007**, 46, 2220 and Inorg. Chem. **2009**, 48, 3288

(5) Werner, P. E.; Eriksson, L.; Westdahl, M. *J. Appl. Crystallogr.* **1985**, *18*, 367–370.

(6) Favre-Nicolin, V.; Černý, R. *J. Appl. Crystallogr.* **2002**, *35*, 734–743.

(7) Larson, A. .; Dreele, R. B. Von *Los Alamos National Laboratory Report* **1994**, 86–748.

(8) Clark, S. J.; Segall, M. D.; Pickard, C. J.; Hasnip, P. J.; Probert, M. I. J.; Refson, K.; Payne, M. C. *Zeitschrift für Kristallographie* **2005**, *220*, 567–570.

(9) Refson, K.; Tulip P. R.; Clark S. J. Phys Rev B, 2006 *73*, 155114.

(10) Ceperley, D. M. *Phys. Rev. Lett.* **1980**, *45*, 566–569.

(11) Perdew, J. P., Zunger, A. *Phys. Rev. B* **1981**, *23*, 5048–5079.

(12) Rappe, A.; Rabe, K.; Kaxiras, E.; Joannopoulos, J. *Phys. Rev. B* **1990**, *41*, 1227–1230.

(13) Morris, A. J.; Nicholls, R. J.; Pickard, C. J.; Yates, J. R. *Comp. Phys. Comm.* **2014**, *185*, 1477.

(14) Baroni, S.; de Gironcoli, S; Dal Corso, A.; Giannozzi, P. *Rev. Mod. Phys.* **2001**, 73, 515–562.

(15) Ramirez-Cuesta, A. J. *Comput. Phys. Commun.* **2004**, *157*, 226–238.

(16) Perdew, J.; Burke, K.; Ernzerhof, M. *Phys. Rev. Lett.* **1996**, *77*, 3865–3868.

(17) Mitchell, P. C. H.; Parker, S. F.; Ramirez-Cuesta, A. J.; Tomkinson J. *Vibrational spectroscopy with neutrons, with applications in chemistry, biology, materials science and catalysis*; World Scientific, 2005.

(18) Parker, S. F.; Fernandez-Alonso, F.; Ramirez-Cuesta, A. J.; Tomkinson, J.; Rudic, S.; Pinna, R. S.; Gorini, G.; Fernández Castañon, J. *Journal of Physics Conference Series*, **2014**, *554*, 012003.

(19) Parker, S. F.; Lennon, D.; Albers, P. W. *Applied Spectroscopy* **2011**, *65*, 1325-1341.

(20) www.isis.stfc.ac.uk.

(21) Parker, S. F. *Coord. Chem. Rev.* **2010**, *254*, 215–234.

(22) Zolliker, P.; Yvon, K.; Fischer, P.; Schefer, J. *Inorg. Chem.* **1985**, *24*, 4177–4180.

(23) Ghosez, P.; Michenaud, J.-P.; Gonze, X. *Phys. Rev. B* **1998**, *58*, 6224.

(24) Verstraete, M.; Gonze, X. *Phys. Rev. B* **2003**, *68*, 195123.

(25) Parker, S. F.; Refson, K.; Williams, K. P. J.; Braden, D. A; Hudson, B. S.; Yvon, K. *Inorg. Chem.* **2006**, *45*, 10951–7.

(26) Parker, S. F.; Jayasooriya, U. A.; Sprunt, J. C.; Bortz, M.; Yvon, K. *Journal of the Chemical Society, Faraday Transactions* **1998**, *94*, 2595–2599.

TOC picture

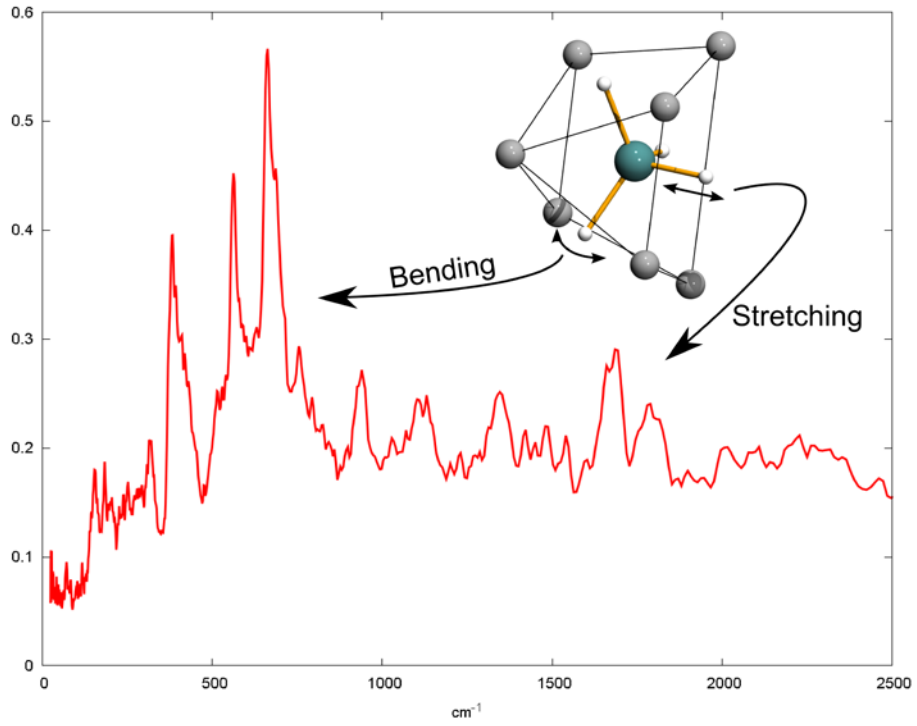
0.6
0.5
0.4
0.3
0.2
0.1
0
0
500
1000
1500
2000
2500
cm-1
Bending
Stretching

Supplementary Information

Stabilization of 3d-transition metal hydrido complexes in $SrH_2Mg_2[Co(I)H_5]$, $BaH_2Mg_5[Co(-I)H_4]_2$ and $RbH_2Mg_5[Co(-I)H_4\ Ni(0)H_4]$ via easily polarizable hydride ligands

Henrik Fahlquist,[1] David Moser,[1$] Dag Noréus,[1] Keith Refson[2] and Stewart F. Parker[3]

[1]Department of Materials and Environmental Chemistry, Arrhenius Laboratory, Stockholm University, S-106 91 Stockholm, Sweden

[2]Computational Science and Engineering Department, STFC Rutherford Appleton Laboratory, Chilton, Didcot, OX11 0QX, UK

[3]ISIS Facility, STFC Rutherford Appleton Laboratory, Chilton, Didcot, Oxon OX11 0QX, UK.

$ Current address: Institute for Renewable Energy, EURAC, 39100 Bolzano, Italy

Table S1. Lattice parameters, atom positions and temperature parameters of $BaD_2Mg_5[Co(\text{-}I)D_4]_2$ in space group *Immm* (71), statistical uncertainties (SU) in parentheses. Experimental values are in normal type, those calculated by CASTEP (for the H-containing species) are in *italics*.

Atom	Wyckoff position	x		y		z		U ($Å^2$)
Ba	2c	0	*0*	0	*0*	½	*½*	0.0018(7)
Co	4e	0	*0*	0.7100(4)	*0.7960*	0	*0*	0.001(1)
Mg1	8n	0.6992(2)	*0.6692*	0.8296(1)	*0.7986*	½	*½*	0.0084(4)
Mg2	2b	0	*0*	½	*½*	0	*0*	0.0246(8)
D1	8m	½	*½*	0.2931(1)	*0.2934*	0.2496(4)	*0.2393*	0.0544(5)
D2	8n	0.6891(2)	*0.6966*	0.8579(1)	*0.8577*	½	*½*	0.0544(5)
D3	4g	0.7932(4)	*0.7974*	0	*0*	0	*0*	0.0544(5)
Lattice parameter (Å)		7.392(2)	*7.2331*	11.602(4)	*11.5250*	4.6265(9)	*4.5641*	

Table S2. Selected distances (<3 Å) and angles for $BaD_2Mg_5[Co(-I)D_4]_2$, statistical uncertainties (SU) in parentheses. Experimental values are in normal type, those calculated by CASTEP (for the H-containing species) are in *italics*.

Atoms	Distance (Å)	
Co-D1 x2	1.504(3)	*1.574*
D2 x2	1.605(3)	*1.590*
D2	2.520(2)	*2.544*
D2-D2	2.799(3)	*2.844*
D3	2.772(2)	*2.712*
D3	2.090(2)	*2.070*
Mg2-D2	2.159(2)	*2.171*
	Angle(deg)	
D1-Co-D1	100.59(9)	*98.25*
D1-Co-D2	108.238(2)	*107.02*
D2-Co-D2	121.33(9)	*126.86*

Table S3a. Metal atom positions and temperature parameters of $RbH_2Mg_5[Co(-I)H_4\ Ni(0)H_4]$, SU in parentheses.

Atom	Wyckoff position	Occupancy	x	y	z	U (Å^2)
Rb	2a	1	0	0	½	0.0109(7)
Co	4d	½	0	0.7032(1)	0.997(1)	0.0019(6)
Ni	4d	½	0	0.7032(1)	0.997(1)	0.0019(6)
Mg1	8e	1	0.7066(3)	0.8300(2)	0.996(3)	0.0267(9)
Mg2	2b	1	0	½	0.878(1)	0.022(2)

Table S3b. Metal atom positions and temperature parameters of $Rb_{0.41}Ba_{0.59}H_2Mg_5[CoH_4]_{1.59}[NiH_4]_{0.41}$, SU in parentheses.

Atom	Wyckoff position	Occupancy	x	y	z	U (Å^2)
Rb	2a	0.41	0	0	½	0.008(1)
Ba	2a	0.59	0	0	½	0.008(1)
Co	4d	0.59	0	0.7054(3)	0.999(6)	0.0042(2)
Ni	4d	0.41	0	0.7054(3)	0.999(6)	0.000(1)
Mg1	8e	1	0.7021(9)	0.8309(5)	0.009(9)	0.015(3)
Mg2	2b	1	0	½	0.932(5)	0.015(7)
Lattice parameter (Å)			7.3811(2)	11.6594(3)	4.6445(1)	

Table S4. Lattice parameters, atom positions and temperature parameters of $SrD_2Mg_2[Co(I)D_5]$, SU in space group $P2_1/m$ (11), parentheses. Experimental values are in normal type, those calculated by CASTEP (for the H-containing species) are in *italics*.

Atom	Wyckoff position	x		y		z		U(Å^2)
Sr	2e	0.7531(8)	*0.7510*	¼	*¼*	0.990(1)	*0.9985*	0.014(1)
Co	2e	0.758(2)	*0.7454*	¼	*¼*	0.499(4)	*0.4836*	0.038(3)
Mg1	2e	0.086(1)	*0.0803*	¼	*¼*	0.621(1)	*0.6240*	0.021(2)
Mg2	2e	0.425(1)	*0.4203*	¼	*¼*	0.373(1)	*0.3702*	0.006(1)
D1	2e	0.0760(6)	*0.0842*	¼	*¼*	0.9127(8)	*0.9227*	0.015(1)
D2	2e	0.5860(6)	*0.5756*	¼	*¼*	0.6398(7)	*0.6536*	0.023(1)
D3	2e	0.4194(7)	*0.4195*	¼	*¼*	0.0876(9)	*0.0733*	0.028(2)
D4	4f	0.6897(4)	*0.6901*	0.0162(9)	*0.4916*	0.3503(6)	*0.3496*	0.031(1)
D5	4f	0.1627(5)	*0.1611*	0.9946(9)	*0.9975*	0.3629(5)	*0.3465*	0.035(2)
Lattice parameter (Å)		7.818(2)	*7.725*	4.462(1)	*4.398*	6.640(2)	*6.467*	β=91.27(2)º *β=91.46º*

Table S5. Selected distances (<3Å) and angles for $SrD_2Mg_2[Co(I)D_5]$, SU in parentheses.

Atoms	Distance(Å)	
Co-D2	1.65(2)	*1.603*
D4 x2	1.52(2)	*1.566*
D5 x2	1.55(2)	*1.568*
D2-D4	2.345(6)	*2.422*
D5	2.204(5)	*2.252*
D5-D5	2.278(6)	*2.177*
D5	2.677(7)	*2.599*
D5	2.153(8)	*2.214*
D5	2.345(8)	*2.320*
	Angle(deg)	
D2-Co-D4	94.9(1)	*99.7*
D2-Co-D5	89.1(1)	*93.4*
D4-Co-D4	86.4(2)	*87.9*
D4-Co-D5	91.8(2)	*91.8*
D5-Co-D5	89.8(2)	*85.5*

Table S6. Lattice parameters, atom positions and temperature parameters of $Mg_2[Co(I)D_5]$, SU in space group *P*4*nmm* (129), SU in parentheses. Experimental values[21] are in normal type, those calculated by CASTEP are in italics.

Atom	Wyckoff position	xyz					
Co	2c	¼	*¼*	¼	*¼*	0.256(2)	*0.2589*
Mg1	2a	¾	*¾*	¼	*¼*	0	*0*
Mg2	2b	¾	*¾*	¼	*¼*	½	*½*
D1	2c	¼	*¼*	¼	*¼*	0.497(2)	*0.4974*
D2	8j	0.4879(4)	*0.4974*	0.4879	*0.4974*	0.2257(3)	*0.2313*
Lattice parameter (Å)		4.463(4)	*4.435*	4.463(4)	*4.435*	6.593(6)	*6.526*

Table S7. Selected distances (<3Å) and angles for $Mg_2[Co(I)D_5]$, SU in parentheses. Experimental values[21] are in normal type, those calculated by CASTEP are in italics.

Atoms	Distance(Å)	
D2	1.515(3)	*1.562*
D1-D2	2.337(9)	*2.354*
D2-D2	2.124(3)	*2.195*
Mg1-D2	2.170(2)	*2.177*
D2	2.402(2)	*2.352*
	Angle(deg)	
D1-Co-D2	97.6(1)	*96.6*
D2-Co-D2	89.1(1)	*89.2*

Table S8. Observed and calculated (at the Γ-point) transition energies with mode descriptions for $BaH_2Mg_5[Co(\text{-}I)H_4]_2$.

Observed / cm^{-1}	Calculated / cm^{-1}	Description
75		Ba translation
97	97	Ba translation + $[Co(\text{-}I)H_4]$ translation
116	145	Mg translation+ $[Co(\text{-}I)H_4]$ libration
146	148	Mg translation+ $[Co(\text{-}I)H_4]$ libration
168	177	Mg translation+ $[Co(\text{-}I)H_4]$ libration
191	21	Mg translation+ $[Co(\text{-}I)H_4]$ translation
218	233	$[Co(\text{-}I)H_4]$ translation
234	241	Mg translation+ $[Co(\text{-}I)H_4]$ translation
249	250	Mg translation
250	268	Mg translation+ $[Co(\text{-}I)H_4]$ translation
279	319	Mg translation
379	395	$[Co(\text{-}I)H_4]$ libration
401	406	$[Co(\text{-}I)H_4]$ libration
408	470	$[Co(\text{-}I)H_4]$ libration
472	526	H–Co–H bend (ν_3 T_2)[a]
554	578	H–Co–H bend (ν_3 T_2)
582	632	H–Co–H bend (ν_3 T_2)
644	644	H–Co–H bend (ν_2 E)
649	672	H–Co–H bend (ν_2 E)[a]
656	712	Interstitial hydride translation
725	733	Interstitial hydride translation
948	958	Interstitial hydride translation
1678	1690	Co–H stretch (ν_3 T_2)
1711	1718	Co–H stretch (ν_3 T_2)
1791	1798	Co–H stretch (ν_3 T_2)
1803	1821	Co–H stretch (ν_1 A_1)

[a] Symmetry classification are for the $[Co(\text{-}I)H_4]^{4-}$ ion in T_d symmetry.[22]

Table S9. Observed and calculated (at the Γ-point) transition energies with mode descriptions for $SrH_2Mg_2[Co(I)H_5]$.

Observed / cm^{-1}	Calculated / cm^{-1}	Description
92	97	Ba translation
102	107	Ba translation
108	118	$[Co(I)H_5]$ translation
157	165	$[Co(I)H_5]$ translation
167	178	$[Co(I)H_5]$ translation
198	211	Mg translation
223	232	Mg translation
235	237	Mg translation
244	254	Mg translation
260	263	Mg translation
279	315	Mg translation
510	545	$[Co(I)H_5]$ libration
547	580	$[Co(I)H_5]$ libration
584	632	$[Co(I)H_5]$ libration
590	616	H–Co–H bend (ν_5 B_1)[a]
582	637	Interstitial hydride translation
670	683	Interstitial hydride translation
761	768	H–Co–H bend (ν_3 A_1)
757	778	Interstitial hydride translation
795	810	Interstitial hydride translation
863	867	H–Co–H bend (ν_8 E)
875	882	H–Co–H bend (ν_8 E)
889	893	H–Co–H bend (ν_9 E)
926	927	H–Co–H bend (ν_9 E)
999	1005	H–Co–H bend (ν_6 B_2)
1035	1042	Interstitial hydride translation
1058	1085	Interstitial hydride translation
1618	1623	Axial Co–H stretch (ν_1 A_1)
1703	1727	Equatorial Co–H stretch (ν_7 E)
1753	1754	Equatorial Co–H stretch (ν_7 E)
1805	1809	Equatorial Co–H stretch (ν_2 A_1)
1815	1818	Equatorial Co–H stretch (ν_4 B_1)

[a]Symmetry classification are for the $[Co(I)H_5]^{4-}$ ion in C_{4v} symmetry.[20,22]

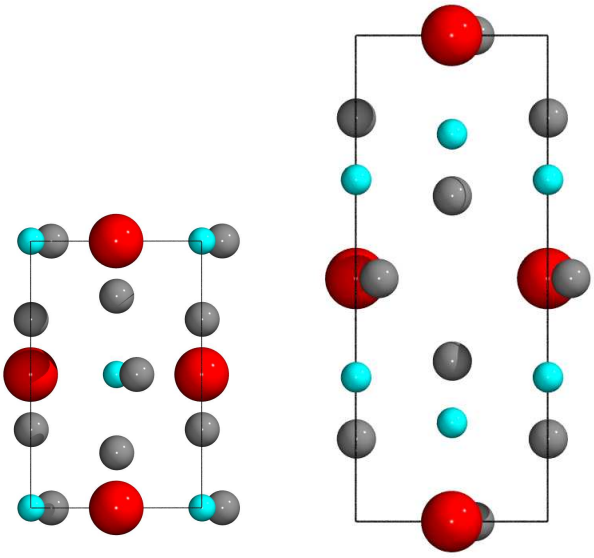

Figure S1. $RbH_2Mg_5[Co(-I)H_4\ Ni(0)H_4]$ Projected in the [100] direction (left) and the [001] direction (right) showing how Mg2 has moved from the position 0.0, 0.5, 0 as Co is exchanged for Ni and Ba is exchanged for Rb. This lowers the symmetry from to *Immm* (71) to *Imm2* (44). Red, cyan, grey spheres denote Rb, Co/Ni and Mg respectively

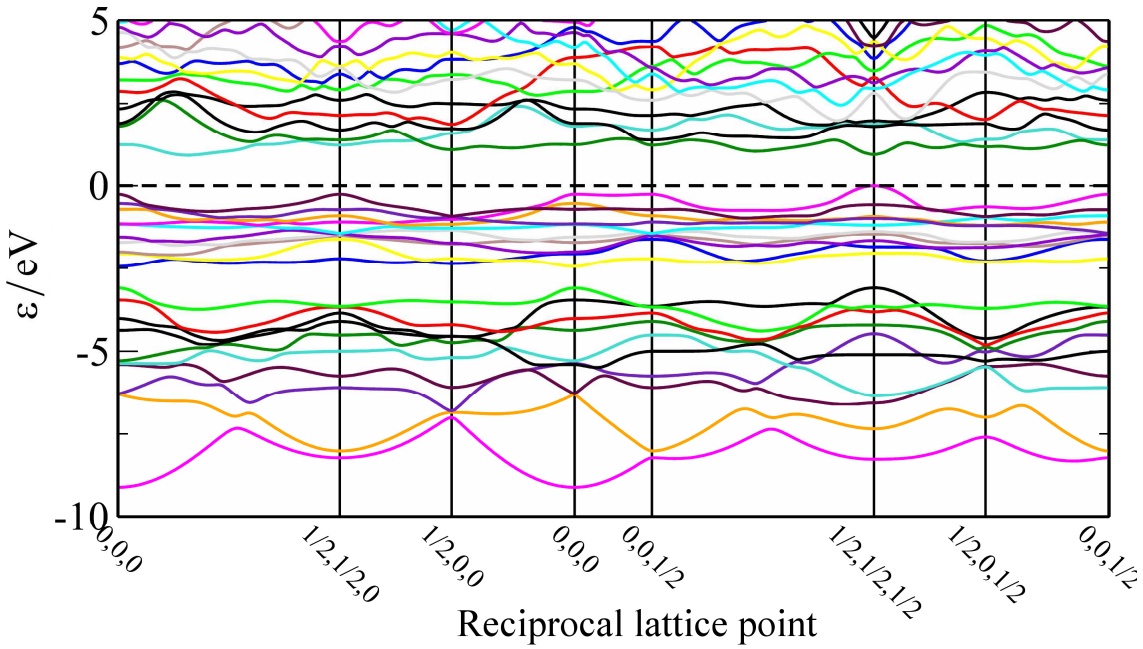

Figure S2. Electronic band structure of $BaH_2Mg_5[Co(-I)H_4]_2$.

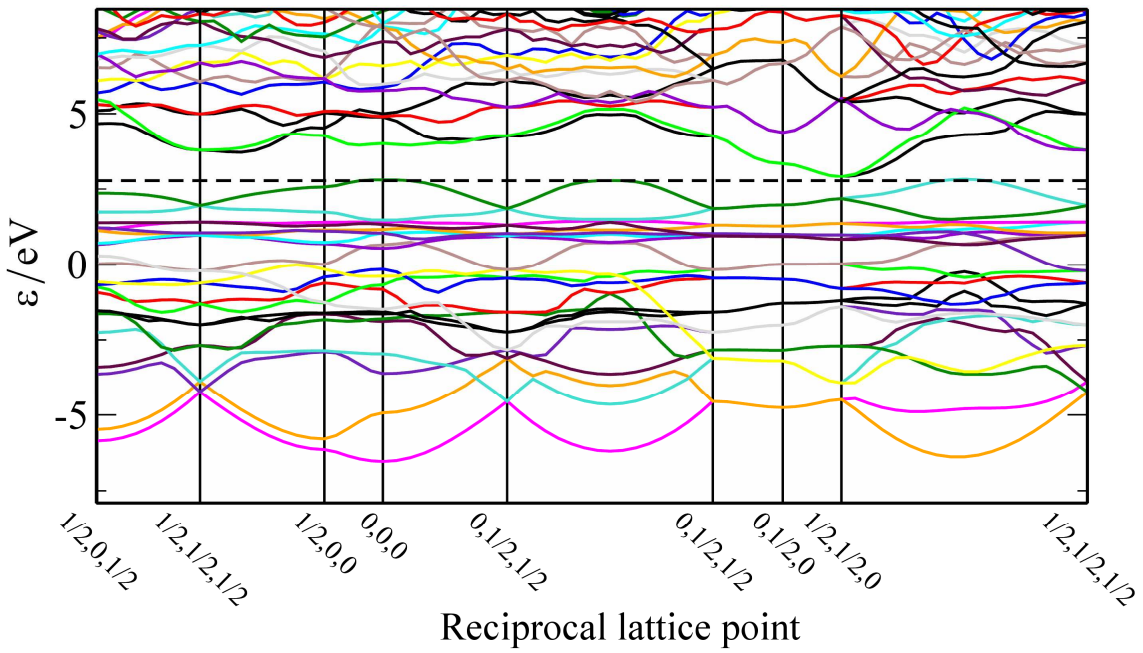

Figure S3 Electronic band structure of $SrH_2Mg_2[Co(I)H_5]$.

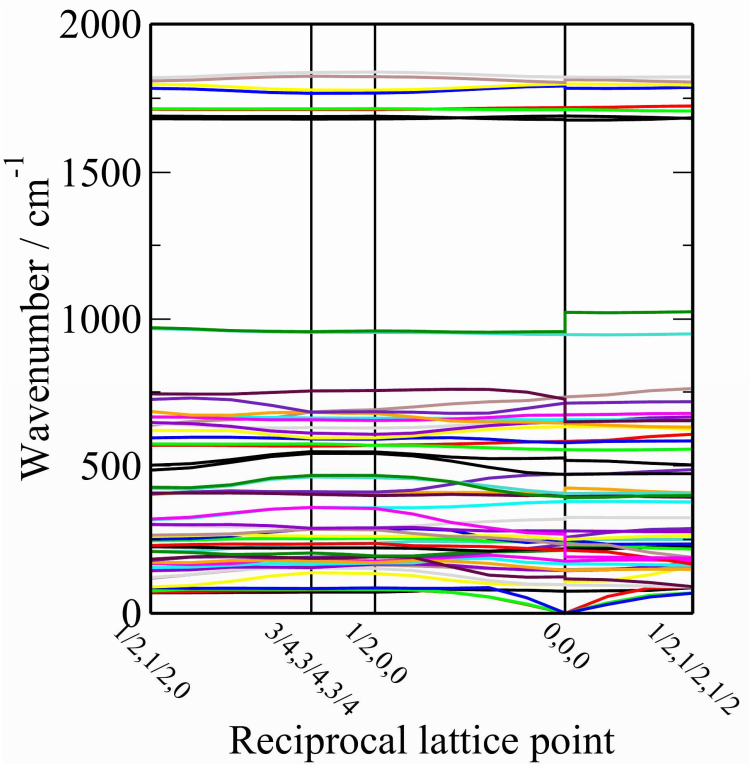

Figure S4. Phonon dispersion curves for $BaH_2Mg_5[Co(-I)H_4]_2$.

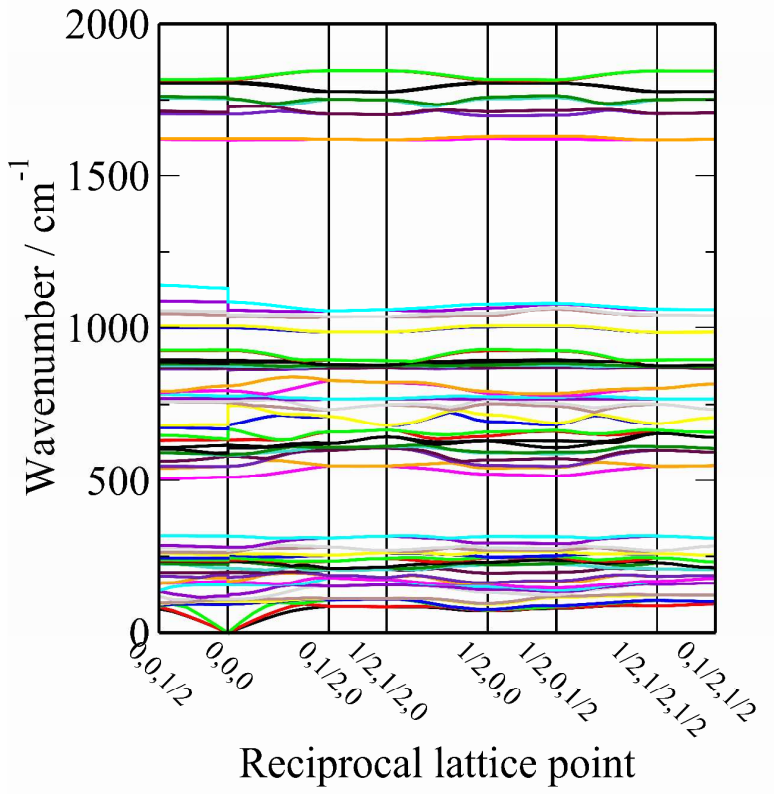

Figure S5. Phonon dispersion curves for $SrH_2Mg_2[Co(I)H_5]$.

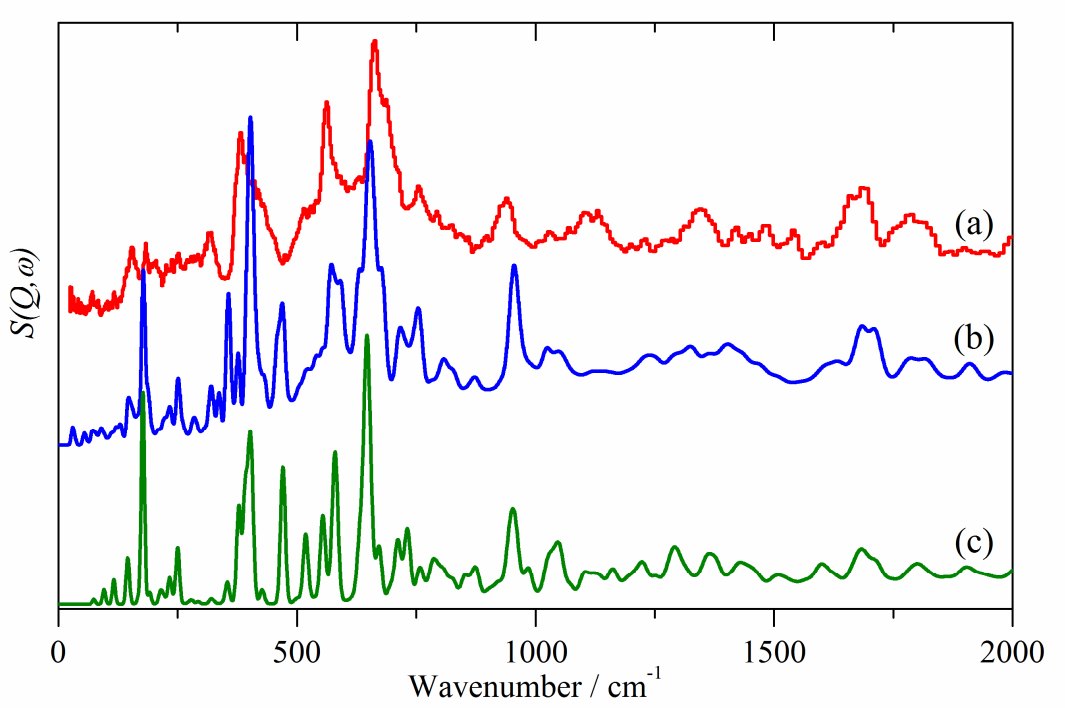

Figure S6. Comparison of INS spectra of $BaH_2Mg_5[Co(\text{-I})H_4]_2$: (a) experimental, (b) generated from the calculation across the entire Brillouin zone and (c) generated from a Γ-point only calculation

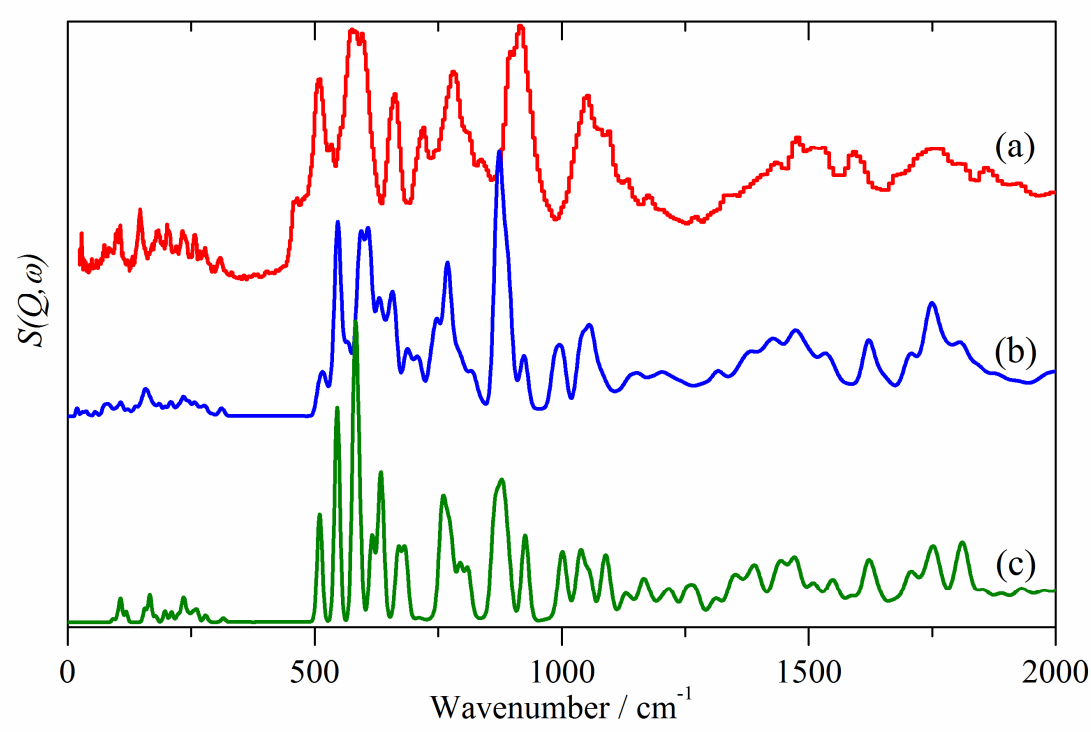

Figure S7. Comparison of INS spectra of $SrH_2Mg_2[Co(I)H_5]$: (a) experimental, (b) generated from the calculation across the Brillouin zone and (c) generated from a Γ-point only calculation